Supporting Information

Boal et al. 10.1073/pnas.0908059106

SI Text

AFM Assays to Measure Protein Redistribution. Additional examples of AFM images used for measurements are provided in Fig. S1.

EndoIII Activity Assays in *E. coli* (CC102). We also performed the experiment where *mutY* is inactivated and the resulting effect on the in vivo activity of EndoIII observed by using CC102, the EndoIII activity reporter strain (Table S1). An average of 14 ± 4 lac^+ revertants were found per 10^9 cells for the CC102 EndoIII activity reporter strain. Upon knocking out *nth* in CC102 (CC102 nth^-), the reversion frequency became 34 ± 8 per 10^9 cells. Removal of *mutY* (CC102 $mutY^-$) led to 27 ± 9 lac^+ revertants. In the double mutant (CC102 $nth^-/mutY^-$), 48 ± 16 revertants were observed. In the CC102 assay, the mutagenesis pathway was likely initiated by damage to cytosine, whereas in the CC104 assay the pathway began with oxidative guanine damage. Because cytosines are far more difficult to oxidize than guanines, especially without imposing oxidative stress on the cells, few cytosine lesions arise spontaneously. Oxidized guanine lesions should be much more prevalent. Thus, there is a significantly higher mutation frequency observed with CC104 $mutY^-$ compared with CC102 nth^-. In addition, the DNA repair assays described here only monitor DNA damage that results in mutation. The primary substrate for MutY is highly mutagenic, whereas the primary substrate for EndoIII (thymine glycol) (1) is less so; hence, these assays may more accurately reflect MutY activity than EndoIII activity inside the cell. Nevertheless, the trend is the same: MutY appears to have a helper function in the EndoIII assay, just as EndoIII seems to have a helper function in the MutY assay. Furthermore, as our model predicts, given their relative copy numbers within the cell, MutY needs more help from EndoIII than vice versa. In fact, the primary role of EndoIII, in the absence of oxidative stress, may be helping MutY.

Note that inactivation of *mutY* or *nth* in *E. coli* did not affect overall cell growth in glucose-supplemented media. Inactivation of *nth* in the MutY activity reporter (CC104) resulted consistently in a 2-fold increase in the mutation rate. In general, inactivation of DNA repair genes in *lacZ*-based mutation reporter strains can yield mutator phenotypes that range from strong to weak (2). Inactivation of MutY itself produced only a moderate increase in the mutation rate (≈15-fold; Table 1). Therefore, it is not surprising that inactivation of a proposed helper of MutY would yield a still smaller effect. Interestingly, despite moderate mutator effect for MutY, the 15-fold change observed when comparing CC104 and CC104/$mutY^-$ corresponded to the difference between 5% and 50% of cells having a transversion somewhere in their genome. Hence, this window is biologically significant, with MutY function spanning a crucial regime for protecting the integrity of the genome from this mutation; within this window, *nth* inactivation holds critical consequences.

Investigation of Y82A EndoIII at an Abasic Site Electrode. Y82A EndoIII was investigated as the purified protein at an electrode modified with a duplex containing an abasic site, a modification known to attenuate DNA-mediated CT to species bound above this lesion. Y82A did not exhibit a signal at this electrode modified with DNA containing an abasic site (Fig. S2), indicating that as with WT EndoIII, oxidation of the [4Fe4S] cluster is DNA-mediated and requires an intact base pair stack.

Supplemental Methods. ***Materials.*** All chemicals were purchased from Sigma–Aldrich. All enzymes were purchased from New England Biolabs unless otherwise specified. All buffers were freshly prepared and filtered before use. Mica surfaces were purchased from SPI Supplies. Silicon AFM probes were purchased from Nanoscience Instruments. Oligonucleotides were purchased from IDT or synthesized on a 3400 DNA synthesizer (Applied Biosystems). All strains used were derivatives of CC104 or CC102 (3) and generated as described below. LB broth was used as the rich medium, whereas NCE (4) medium supplemented with $MgSO_4$ (100 μM) and glucose (11 mM) or lactose (6 mM) was used as the minimal medium.

Genome scanning calculations. The time for sliding to scan the genome is calculated from a 1D random walk (5). The 1D diffusion (sliding) constant has been measured (6) in vitro for the DNA repair proteins hOGG1 and *Bacillus stearothermophilus* MutM as 5×10^6 bp^2/s and 3.5×10^5 bp^2/s, respectively. Taking the more generous (faster) value for the diffusion constant, a genome size of 5×10^6 bp, and the MutY copy number of 30 yields a scanning time of 46 min. Short hops have been found (5) to have an insubstantial effect on the total search time. This result is consistent with the analysis of Wunderlich and Mirny (7). The tight 10^{-7} K_d of MutY for undamaged DNA 30-mers corresponds to greater than 99.99% bound protein in vivo, inconsistent with facile 3D translocation (8).

We can calculate the step time for 3D diffusion of the reduced protein to the DNA as

$$t = \frac{V}{k_a C_p(1 - \Theta)}, \qquad [1]$$

where V is the cell volume, $C_p(1 - È)$ is the number of reduced repair proteins in the volume (È = fraction oxidized), and k_a is the bimolecular rate constant for protein association with the DNA target within the cellular volume. The bimolecular rate constant can be determined by using a modified Smoluchowski equation for protein collision with a rod of DNA within the cell volume, where the length of the rod is twice the number of bases, N, over which DNA-mediated CT can proceed, because reduced protein can transfer an electron from either side. Any contact of the reduced protein within the DNA rod allows electron transfer to the DNA-bound oxidized protein. We assume that DNA is a rod over a region $2N$ base pairs long, but clearly the organization of the bacterial nucleoid is more complex (9). The Smoluchowski equation is constructed with two terms: one describes the ballistic 3D diffusion of the reduced protein to the DNA, and the second (10) considers the gyrations of a rod with persistence length of 150 bp and the ends fixed as part of the chromosome.

$$k_a = 4\pi\kappa f D_p\,(rDNA + r_p) + D_a\, a\, \sqrt[3]{\frac{rDNA + r_p}{a}}. \qquad [2]$$

The protein diffusion constant (D_p) is determined from the Stokes–Einstein equation using the 10-cP viscosity of *E. coli* cytoplasm (11) and the measured Stokes radius of EndoIII (r_p) (12). DNA diffusion is considered to be negligible. The persistence length of DNA (150 bp) is defined as a. The electrostatic (f) and orientational (κ) constants are taken as unity (13), in keeping with the high ionic strength in vivo environment. The dissociation rate of the protein is not included in our model because charge equilibration should occur on a much faster timescale than dissociation of the reduced protein; implicitly, the

dissociation rate is incorporated into the parameter for the maximum distance of charge transport before dissociation, N. Note that the reduced protein is not allowed here to exploit facilitated search to colocalize with the oxidized protein. We also make no distinction between 5′ to 3′ versus 3′ to 5′ transport, although subtle differences have been observed (14). We can calculate the overall time to search the genome of Z bases through the random walk of the electron as

$$T_{ox} = t\left(\frac{4Z}{N}\right)^2. \quad [3]$$

Because there is equal probability of reduced protein associating with each base in the CT-active target region, and N represents that maximum distance of interprotein charge transfer, the average distance of interprotein CT is $N/2$. Self-exchange decreases the average step distance by a further factor of 2.

This represents the scanning time for a single oxidized protein. Each oxidized protein provides a separate nucleation site for CT scanning but draws from the same reservoir of reduced protein to scan different portions of the genome,

$$T_{CT} = t\left(\frac{4Z}{\Theta C_p N}\right)^2. \quad [4]$$

Scanning through sliding without a CT search represents a boundary condition, so that the total time is

$$T = (T_{CT}^{-1} + T_D^{-1})^{-1} \quad [5]$$

where T_D is the diffusion scanning time.

Generation of DNA samples for AFM. Four primers were synthesized with the following sequences:

5′-GTACAGAGTTCAGTCGGCATCCGCTTA-CAGACAAGC-3′ (forward),

5′-CCGGTAACTATCGTCTTGAGTCC-3′ (reverse),

5′-GACTGAACTCTGTACCTGGCACGACAG-GTTTCCCG-3′ (forward), and

5′-GACTGAACTCTATACCTGGCACGACAG-GTTTCCCG-3′ (forward).

The underlined bases highlight the location of a 2′-*O*-methyl residue (15). These primers were used in separate PCR reactions using pUC19 as a template to generate three duplexes 1610 bp, 2157 bp (matched), or 3767 bp (mismatched) long and each containing one 14-nucleotide single-strand overhang. These PCR products were purified by ethanol precipitation and resuspended in 50 mM NaCl and 5 mM sodium phosphate (pH 7) buffer and quantitated by OD_{260}. Duplexes were phosphorylated by using 100 units of PNK in 10% T4 DNA ligase buffer for 1 h at 37 °C and were deactivated for 10 min at 65 °C. Separate duplexes were annealed at 65 °C for 8 min, then cooled to 20 °C during 2 h. The resulting larger duplexes were ethanol-precipitated and resuspended in 100 μL of 50 mM NaCl/5 mM phosphate buffer. A total of 15 units of T4 DNA ligase and 10% T4 ligase buffer were added (total reaction volume ≈150 μL) and incubated overnight at 16 °C, followed by deactivation for 10 min at 65 °C. We did not bring the ligation reaction to completion, so as to obtain a mixture of DNA samples that were equivalent other than the presence of the mismatch at the ligation site. The DNA duplexes (ligated and unligated) were then analyzed by 0.6% agarose gel electrophoresis. The strategy for preparation of samples is given in Fig. S4.

AFM deposition conditions. Mica surfaces were freshly cleaved with scotch tape. EndoIII (0.4 μM) was added to the stock DNA solution containing 50–100 ng of total DNA composed of the mixture of ligated 3.8-kb duplexes and the two unligated duplexes (1.6 and 2.2 kb) in 6 mM $MgCl_2$/Tris-EDTA buffer. This protein–DNA solution was incubated at 4 °C overnight and deposited (5 μL) on the mica surface for 2 min, rinsed with 2 mL of water, and dried under argon. To study the effects of protein oxidation, protein–DNA solutions were treated with 1 or 5 μM H_2O_2, incubated for 2 min, and deposited onto the mica surface as described. Two of the five WT EndoIII samples analyzed were deposited onto the mica surface in 5-ng quantities, followed by immediate addition of 3.7 μM EndoIII (1-μL volume). This difference in deposition conditions did not result in any significant differences in the trends observed. Mutant protein (Y82A) was added to a stock solution of 50 ng of DNA for a final protein concentration of 0.4 μM. After incubation at 4 °C overnight, deposition conditions were identical to that for WT EndoIII-DNA samples.

AFM instrument setup. Silicon AFM Probes purchased from Nanoscience Instruments (BudgetSensors), with a spring constant of 3 N/m and a resonance frequency of 75 kHz, were used in a Digital Instruments Multimode SPM. Images with scan areas of 2×2 μm^2 or 1×1 μm^2 were acquired in tapping mode by using an amplitude of 0.5416–0.200 V at a scan rate of 3.05 Hz. Scan rates of 3.05 Hz were used to obtain images of higher quality. Data analysis was performed by using the WSxM program (16). Strands and proteins were counted as described in the main text.

Strain construction. CC104 and CC102 strains were generously donated (3), as was CC104 *mutY*$^-$ (CC104 *muty*::minitn 10) (17). The *nth* was replaced with a chloramphenicol-resistance cassette (*cm*) in CC104 and CC104 *mutY*$^-$ by using a previously described in-frame deletion method (18). See Table S4 for primer sequences; *nth* homology regions are shown in regular text, and *cm* priming regions are highlighted in boldface. CC102 strains were constructed by using P1 transduction (19). Inactivation in all strains was verified with colony PCR.

lac*$^+$ reversion assays. Strains were streaked to LB medium and incubated overnight at 37 °C. For *nth* knockouts, strains were streaked to LB plus chloramphenicol (17 μg/mL), and for *mutY* knockouts, strains were streaked to LB plus tetracycline (50 μg/mL). A total of 1 mL of LB culture was started from single colonies and grown overnight in a shaking incubator at 37 °C, 220 rpm. A total of 20 μL of each starter culture was used to inoculate a 10-mL NCE plus glucose culture, which was then grown to a density of 10^9 cells per milliliter at 37 °C, 250 rpm. Cell density was determined by dilution plating a 10-μL aliquot of the NCE plus glucose culture onto NCE plus glucose solid medium, followed by incubation at 37 °C for 36 h. A total of 5 mL of this culture was centrifuged in a clinical tabletop centrifuge at 4 °C and plated on NCE plus lactose solid medium and then incubated at 37 °C for 36 h. Colonies arising are reported as *lac*$^+$ revertants per milliliter of cells plated. In experiments incorporating plasmid vectors, CC104 and CC102 strains were made electrocompetent (19) and transformed via electroporation at 1.8 kV. Transformants were selected on LB plus ampicillin (amp; 100 μg/mL) solid medium after incubation overnight at 37 °C. Single colonies were restreaked to LB plus amp (100 μg/mL) solid media and incubated for 12 h at 37 °C. A total of 1 mL of LB plus amp (100 μg/mL) cultures was started from these colonies and grown overnight at 37 °C, 220 rpm. A total of 20 μL of this starter culture was used to inoculate a 10-mL NCE plus glucose plus amp (40 μg/mL) culture, which was grown to a density of 10^9 cells per milliliter at 37 °C, 250 rpm. A total of 5 mL of this culture was plated onto NCE plus lactose plus amp (40 μg/mL) and incubated at 37 °C for 36 h. The *lac*$^+$ revertants were reported as described above. Exposure to ampicillin increases the number of revertants.

Mutagenesis. The *nth* was cloned into pBBR1MCS-4(p) by using standard techniques (20). Primer sequences are given in Table S4; restriction sites are highlighted in boldface. Gene incorporation was verified by PCR and sequencing (Laragen) using KS/SK (pBBR1MCS-4-derived vectors) or M13 (pNTH10-derived vectors) sequencing primers. Mutants were generated by

using a QuikChange site-directed mutagenesis kit (Stratagene) and verified by three independent sequencing reactions (Laragen). Primers used are shown in Table S4; the altered codon site is highlighted in boldface.

Protein expression and purification. EndoIII and Y82A EndoIII were expressed from the pNTH10 expression vector and purified as described previously (21). Protein concentrations were determined by using the UV–visible absorbance of the [4Fe4S] cluster (410 nm; ε = 17,000 $M^{-1}{\cdot}cm^{-1}$) (22).

Glycosylase assays. Oligonucleotides were synthesized containing a 5-OH-dU lesion site (purchased as a phosphoramidite from Glen Research), HPLC-purified, and verified with MALDI-TOF mass spectrometry. The following sequences were used: 5′-TGTCAATAGCAAGXGGAGAAGTCAATCGTGAGTCT-3′ plus complementary strand, where X = 5-OH-dU base-paired with G. The strand containing the lesion was 5′-^{32}P-end-labeled as described previously (20) and annealed to its complement. Reactions were run at 37 °C for 15 min with 10 nM DNA and 100 or 10 nM protein and were quenched with 1 M NaOH (23). Samples were analyzed by denaturing 20% PAGE and imaged by autoradiography. Band intensity was quantified by using ImageQuant software (GE Healthcare).

Electrochemistry at DNA-modified electrodes. DNA-modified electrodes for protein electrochemistry experiments were prepared as described previously (24) by using the following sequences: thiol-modified strand, 5′-AGTACAGTCATCGCG-3′; TA complementary strand, 5′-CGCGATGACTGTACT-3′; and abasic site (Ab) complementary strand, 5′-CGCGATGACTGTXCT-3′, where X = dSpacer (Glen Research). Surfaces were backfilled with 1 mM mercaptohexanol for 30 min and rinsed at least three times with protein storage buffer [20 mM sodium phosphate, 100 mM NaCl, 0.5 mM EDTA, and 20% glycerol, (pH 7.5)]. Protein solution was introduced to the electrode surface and allowed to incubate for ≈20 min until signal reached full intensity. Cyclic voltammetry experiments were performed on a CH Instruments 760 potentiostat using a 50-mV/s scan rate, Ag/AgCl reference electrode, and Pt wire auxiliary electrode in an electrochemical cell modified for protein experiments (24).

1. Kuo CF, et al. (1995) Atomic structure of the DNA repair [4Fe-4S] enzyme endonuclease III. *Science* 258:434–440.
2. Miller JH (1996) Spontaneous mutators in bacteria: Insights into pathways of mutagenesis and repair. *Annu Rev Microbiol* 50:625–643.
3. Cupples CG, Miller JH (1989) A set of *lacZ* mutations in *Escherichia coli* that allow rapid detection of each of the six base substitutions. *Proc Natl Acad Sci USA* 86:5345–5349.
4. Davis, RW, Botstein D, Roth, JR (1980) *Advanced Bacterial Genetics*: *A Manual for Genetic Engineering* (Cold Spring Harbor Lab Press, Cold Spring Harbor, NY).
5. Berg OG, Winter RB, von Hippel PH (1981) Diffusion-driven mechanisms of protein translocation on nucleic acids. 1. Models and theory. *Biochemistry* 20:6929–6948.
6. Blainey PC, van Oijen AM, Banerjee A, Verdine GL, Xie XS (2006) A base-excision repair protein finds intrahelical lesion bases by fast sliding in contact with DNA. *Proc Natl Acad Sci USA* 103:5752–5757.
7. Wunderlich Z, Mirny LA (2008) Spatial effects on the speed and reliability of protein-DNA search. *Nucleic Acids Res* 36:3570–3578.
8. Porello SL, Williams SD, Kuhn H, Michaels ML, David SS (1996) Specific recognition of substrate analogs by the DNA mismatch repair enzyme MutY. *J Am Chem Soc* 118:10684–10692.
9. Thanbichler M, Wang SC, Shapiro L (2005) The bacterial nucleoid: A highly organized and dynamic structure. *J Cell Biochem* 96:506–521.
10. Berg OG (1986) Effective diffusion rate through a polymer network: Influence of nonspecific binding and intersegment transfer. *Biopolymers* 25:811–821.
11. Mullineaux CW, Nenninger A, Ray N, Robinson C (2006) Diffusion of green fluorescent protein in three cell environments in *Escherichia coli*. *J Bacteriol* 188:3442–3448.
12. Asahara H, Wistort PM, Bank JF, Bakerian RH, Cunningham RP (1989) Purification and characterization of *Escherichia coli* endonuclease III from the cloned *nth* gene. *Biochemistry* 28:4444–4449.
13. Berg OG, von Hippel PH (1985) Diffusion-controlled macromolecular interactions. *Annu Rev Biophys Chem* 14:131–160.
14. O'Neill MA, Barton JK (2002) Effects of strand and directional asymmetry on base-base coupling and charge transfer in double-helical DNA. *Proc Natl Acad Sci USA* 99:16543–16550.
15. Donahue WF, Turczyk BM, Jarrell KA (2002) Rapid gene cloning using terminator primers and modular vectors. *Nucleic Acids Res* 30:e95.
16. Horcas I, et al. (2007) WSXM: A software for scanning probe microscopy and a tool for nanotechnology. *Rev Sci Instrum* 78:013705.
17. Golinelli MP, Chmiel NH, David SS (1999) Site-directed mutagenesis of the cysteine ligands to the [4Fe4S] cluster of *Escherichia coli* MutY. *Biochemistry* 38:6997–7007.
18. Datsenko KA, Wanner BL (2000) One-step inactivation of chromosomal genes in *Escherichia coli* K12 using PCR products. *Proc Natl Acad Sci USA* 97:6640–6645.
19. Miller JH (1992) *A Short Course in Bacterial Genetics*: *A Laboratory Manual and Handbook for Escherichia coli and Related Bacteria* (Cold Spring Harbor Lab Press, Cold Spring Harbor, NY).
20. Sambrook J, Russell DW (2001) *Molecular Cloning: A Laboratory Manual* (Cold Spring Harbor Lab Press, Cold Spring Harbor, NY).
21. Boiteux S, O'Connor TR, Laval J (1987) Formamidopyrimidine-DNA glycosylase of *Escherichia coli*: Cloning and sequencing of the *fpg* structural gene and overproduction of the protein. *EMBO J* 6:3177–3183.
22. Cunningham RP, et al. (1989) Endonuclease III is an iron-sulfur protein. *Biochemistry* 28:4450–4455.
23. Watanabe T, Blaisdell JO, Wallace SS, Bond JP (2005) Engineering functional changes in *Escherichia coli* endonuclease III based on phylogenetic and structural analyses. *J Biol Chem* 280:34378–34384.
24. Boal AK, et al. (2005) DNA-bound redox activity of DNA repair glycosylases containing [4Fe4S] clusters. *Biochemistry* 44:8397–8407.

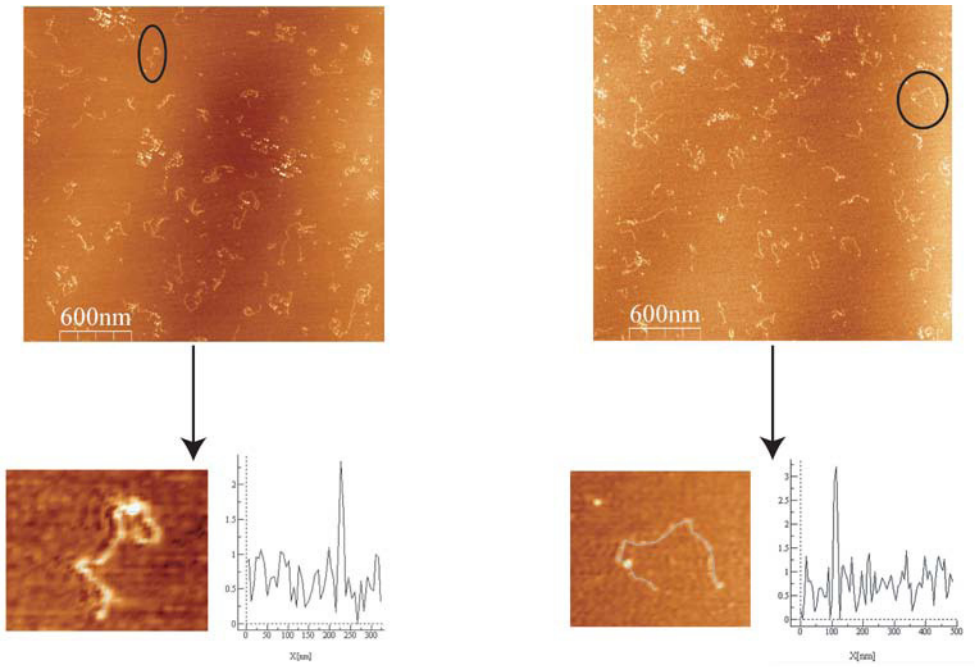

Fig. S1. (*Upper*) Tapping-mode AFM images of DNA and EndoIII protein on mica imaged in air. DNA (strands) and protein (dots) are visible on the surface. Images were acquired with a scan size of 3×3 μm^2, at a rate of 3.05 Hz, with a data scale of 10 nm. (*Lower*) Zoomed-in images of a DNA strand with a bound protein subjected to height profiling to distinguish protein. The profile of the strand, to the right of the zoomed-in image, shows that the height of DNA ranges from 1 to 2 nm, with a much higher (>2 nm) protein peak.

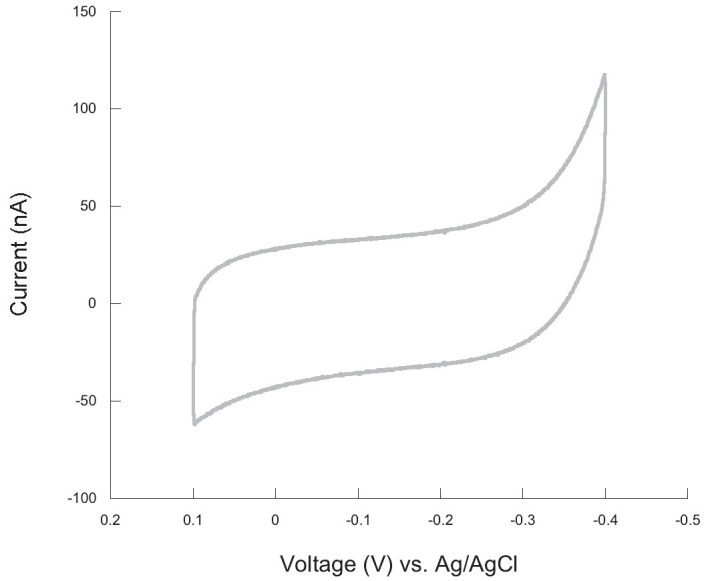

Fig. S2. Y82A EndoIII examined by cyclic voltammetry at an Au electrode surface modified with DNA containing an abasic site. No peak is evident, indicating that CT to the [4Fe4S] cluster in Y82A EndoIII requires an intact DNA π-stack.

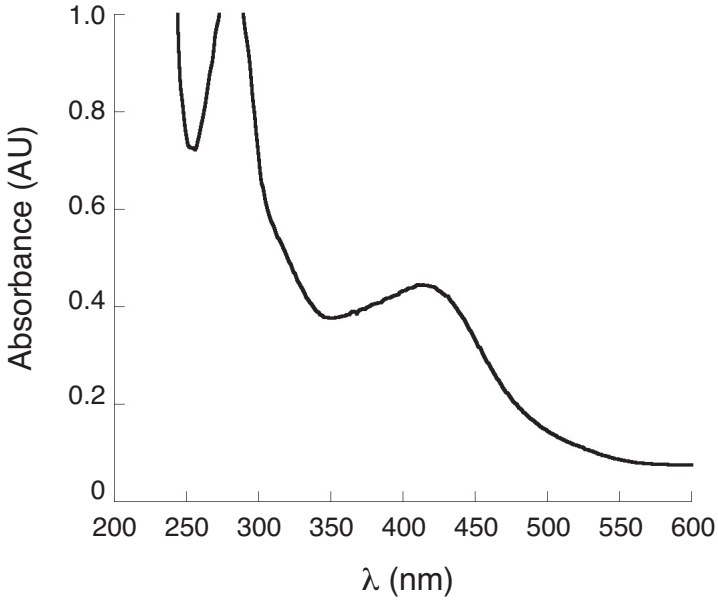

Fig. S3. The UV-visible spectrum of Y82A EndoIII. A peak in the visible region is observed at 410 nm, characteristic of a [4Fe4S] cluster.

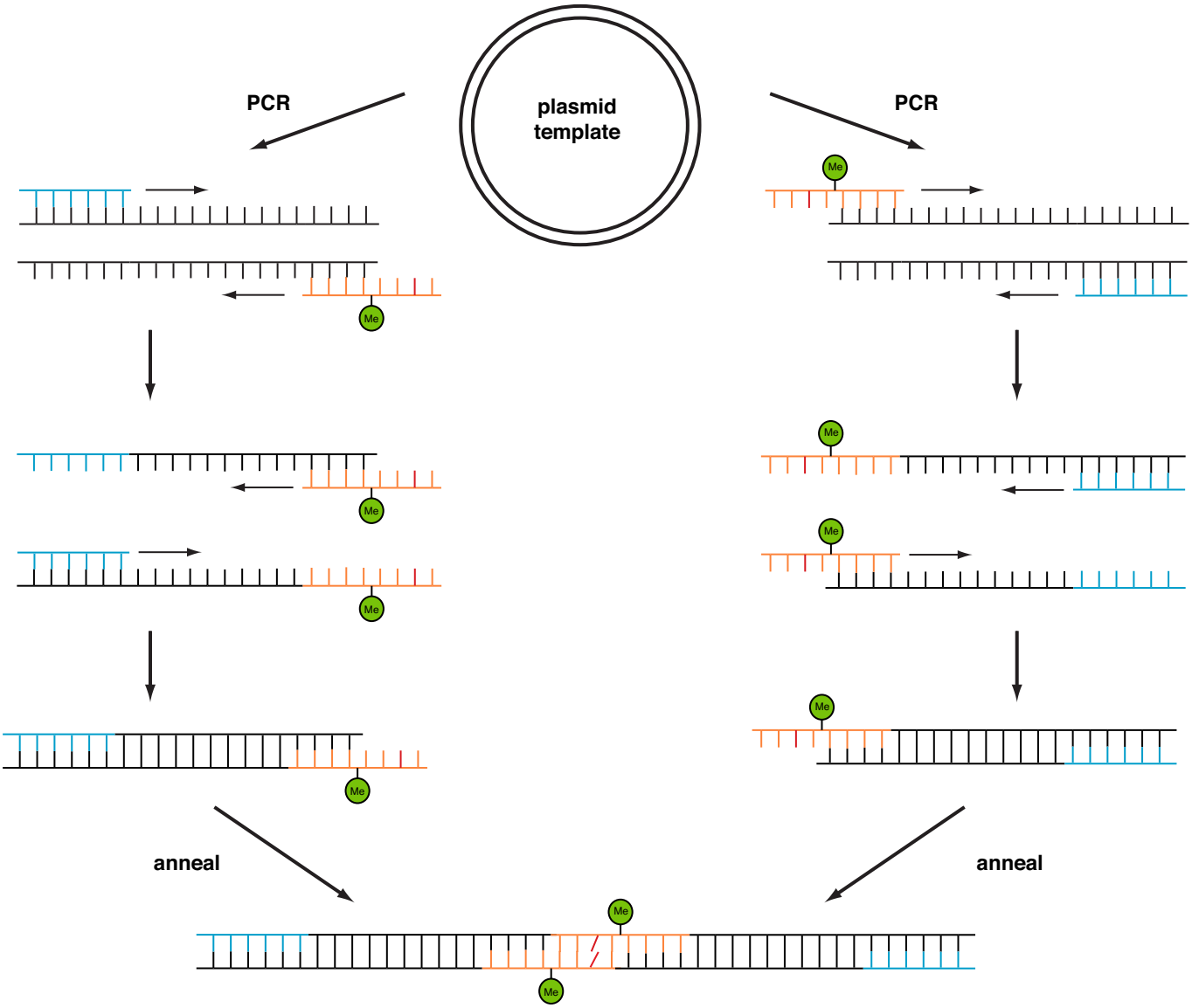

Fig. S4. Two synthesized primers, one incorporating a 2′-*O*-methyl ribonucleotide (blue and orange, respectively), are used to amplify plasmid sequences via PCR. A nucleotide is incorporated within the synthesized primer containing the 2′-*O*-methyl ribonucleotide (orange) that will result in a mismatched or matched final product. As the vector is amplified, polymerase stops at the ribonucleotide (green), resulting in a large single-strand overhang. On performing two separate PCRs with two primers each (orange and blue), the resulting duplexes with 14-bp single-strand overhangs can be annealed/ligated together in good yield to produce long duplexes with or without a mismatch.

Table S1. Assay for DNA repair in *E. coli* by EndoIII (CC102)

Strain	*lac*$^+$ revertants*	Increase, *x*/CC102
CC102†	14 ± 4	—
CC102 *nth*$^-$	34 ± 8	2.4
CC102 *mutY*$^-$	27 ± 9	1.9
CC102 *mutY*$^-$/*nth*$^-$	48 ± 16	3.4

*The *lac*$^+$ revertants are reported as the average number of *lac*$^+$ colonies that arise per 10^9 cells plated on minimal lactose medium. These data represent a single set of experiments, with 10 replicates per strain assayed concurrently.
†CC102 strains reflect the rate of GC-to-TA transversion mutations and serve as a reporter for MutY activity in *E. coli*.

Table S2. MutY activity assay (CC104) with an enzymatic EndoIII mutant (D138A)

Strain	*lac*$^+$ revertants*	Increase, *x*/CC104/p
CC104/p†	33 ± 2.0	—
CC104 *nth*$^-$/p	64 ± 7.4	1.9
CC104 *nth*$^-$/pnth	36 ± 3.3	1.1
CC104 *nth*$^-$/D138A	32 ± 3.2	1.0

Control experiments, including an empty vector p or a vector containing WT *nth* (pnth), are also shown.

*The *lac*$^+$ revertants are reported as the average number of *lac*$^+$ colonies that arise per 10^9 cells plated on minimal lactose medium with ampicillin (40 μg/mL). These data represent a single set of experiments, with 10 replicates per strain assayed concurrently.

†CC104 strains reflect the rate of GC-to-TA transversion mutations and serve as a reporter for MutY activity in *E. coli*.

Table S3. EndoIII activity assay (CC102) with an enzymatic EndoIII mutant (D138A) and a DNA CT mutant (Y82A)

Strain	*lac*$^+$ revertants*	Increase, *x*/CC102/p
CC102/p†	10 ± 4.2	—
CC102 *nth*$^-$/p	68 ± 26	6.8
CC102 *nth*$^-$/pnth	18 ± 5.4	1.8
CC102 *nth*$^-$/D138A	62 ± 31	6.2
CC102 *nth*$^-$/Y82A	16 ± 7.1	1.6

Control experiments, including an empty vector p or a vector containing WT *nth* (pnth), are also shown.

*The *lac*$^+$ revertants are reported as the average number of *lac*$^+$ colonies that arise per 10^9 cells plated on minimal lactose media with ampicillin (40 μg/mL). These data represent a single set of experiments, with 10 replicates per strain assayed concurrently.

†CC102 strains reflect the rate of GC-to-AT transition mutations and serve as a reporter for EndoIII activity in *E. coli*.

Table S4. Primer sequences used for *nth* activation, cloning, and mutagenesis

Function	Primer sequence
Wanner inactivation of *nth*	5′-gaagcagctgcagaacgtgcattgccaaacggtgaaacagggaatgtctg**ggtgtaggctggagctgcttc**-3′
	5′-agaggataaagaaaggttatcaatggggtaatcggtgttacccctttttct**catatgaatatcctccttag**-3′
Cloning *nth* into pBBR1MCS-4	5′-**ggaattc**gcaatggcacattgtttgac-3′
	5′-**aggttcct**caatggggtaatcggtgtt-3′
D138A mutant generation	5′-cggctggccgactattgctgtc**gc***cacgcacattttccgcg-3′ plus complement
Y82A mutant generation	5′-ggggtgaaaacctatatcaaaactattgggcttgctaacagcaaagc-3′ plus complement

nth homology regions are shown in regular text, and *cm* priming regions are highlighted in boldface.
*The altered codon site is highlighted in boldface.